Two-Photon Nanolithography Enhances the Performance of an Ionic Liquid–Polymer Composite Sensor

*Natalia A. Bakhtina, Ute Loeffelmann, Neil MacKinnon, and Jan G. Korvink**

Continuous development of fabrication technologies, such as two-photon polymerization (2PP), allows the exact reconstruction of specific volume shapes at micro- and nanometer precision. Advancements in the engineering of new materials, such as ionic liquids (ILs), are bringing superior advantages in terms of material characteristics, facilitating a combination of optical and electrical properties, as well as lithographic capabilities. In this paper, 2PP is utilized for structuring of a novel IL–polymer composite in a single-step manufacturing process with high resolution, down to 200 nm, and high aspect ratio, up to 1:20. The composition, based on a photosensitive photoresist (e.g., IP-L 780 or SU-8) and the IL 1-butyl-3-methylimidazolium dicyanamide, possesses a good ionic conductivity (in the range of 1–10 mS cm^{-1}) over a wide frequency bandwidth (1 kHz–1 MHz), an electrochemical window of 2.7 V, and a good optical transparency (transmission value of 90% for a 170 µm thick film). The fabricated structures are characterized and the phenomenon of enhanced conductivity (up to 4 S cm^{-1}) is explained. Two potential applications, including temperature and relative humidity sensing, are demonstrated as examples. The results suggest a new advanced approach for material structuring that can be regarded as highly most promising for a wide range of applications.

1. Introduction

Lithography is a well established technology for the fabrication of microelectrical–mechanical system (MEMS) devices. During this process different patterns are transferred from the photolithographic mask to a layer of light-sensitive material, i.e., a photoresist, employing an energy source (e.g., UV-light). Important aspects of the lithography technology are feature size and manufacturing cost (i.e., materials, number of photomasks, etc.).

Conventional photolithography is developing in the direction of increasing resolution while decreasing fabrication costs. Ultimately, the resolution of the structures is mainly dictated by the diffraction limit of the radiation used. Thus, a disadvantage of conventional techniques is the inability to fabricate structures with feature sizes below 50 nm.[1] As a result of this fundamental limitation, several alternative approaches have been explored. Electron-beam (e-beam) lithography is one method used to obtain higher resolutions (below 30 nm). A focused e-beam initiates the polymerization of the photoresist, thus no photomask is required. However, this patterning method is limited by the size of the exposed lithographic area.[2] Furthermore, the process is not suitable for mass-production since it is a relatively slow technology, and the e-beam stability becomes problematic during the time consuming writing process. Alternatively, X-ray lithography is a further nanotechnology in which exposure wavelengths of under 100 nm are used and structures smaller than 30 nm may be achieved.[3] Unfortunately, the high costs of mask fabrication for X-ray lithography limits the implementation of this technology in large scale production. For low-cost pattern imprinting, nanoimprint lithography can be used. This method uses a molding or a stamping process to replicate patterns from a master. Structures with dimensions in the range of 10 nm have been presented.[1] Two difficulties restrict the wide spread use of nanoimprinting: the generation of the mold (it must be patterned by another method, for example, those discussed above) and low replication yields.

As the range of scientific and industrial applications has been increasing, the requirements on the materials and their processing have become more challenging. For example, all these lithographic methods, which use masks or expose directly the photoresist material, are limited to planar processing. Therefore, manufacturing of 3D structures requires a flat surface to start with and a multistep chemical posttreatment.

To overcome this processing limitation, further development in the engineering of new fabrication technologies and materials is required to extend device functionalities to applications requiring 3D microstructures. For instance, two-photon polymerization (2-PP), also known as 3D direct laser writing (DLW) lithography, is a novel rapid prototyping technique that permits the fabrication of complex volume structures with a feature size below 100 nm, i.e., much smaller than the irradiated wavelength of the light.[4] The key aspect of this method is that polymerization takes place only inside the focus of the laser beam. Thus, the 2-PP process provides a one-step 3D patterning approach and a superior nanometer resolution in combination with an accurate control of the topology.[5]

N. A. Bakhtina, Dr. U. Loeffelmann, Dr. N. MacKinnon,
Prof. J. G. Korvink
Laboratory for Simulation
IMTEK – Department of Microsystems Engineering
University of Freiburg
Georges-Koehler-Allee 103, 79110 Freiburg, Germany
E-mail: korvink@imtek.uni-freiburg.de

DOI: 10.1002/adfm.201404370

The process diversity and the adaptability of the 2-PP fabrication technique are significantly determined by the properties of the employed photoresist. For example, IP-L 780 (Nanoscribe GmbH, Germany) is a solvent-free negative photoresist formulation, designed specifically for the demands of two-photon absorption, that allows extraordinary 3D resolution and high mechanical stability.[6] No pre- and postexposure thermal treatment is required for solvent removal and chemical curing of the material, respectively. Thus, IP-L 780 is ideally suited for fast automated processes, as the curing process can be exactly controlled in spatial and temporal terms and takes place within seconds without heating of the material. Other advantages of the photoresist are a low proximity effect, little shrinkage, good adhesion on glass substrates, and easy handling (e.g., drop-casting of the photoresist). The 2-PP-induced curing of IP-L 780 results in a change in the refractive index compared to uncured resin. This allows a visual observation of the curing and makes IP-L 780 extremely suitable for real-time optimization of the fabrication process.

Generally, photoresist is an electronic insulator in its pure (i.e., undoped) state. In order to significantly increase the conductivity of the polymerized material, other composites, such as terthiophene (3T) with copper (II) perchlorate,[7] carbon black particles,[8] silver or protonically doped polyaniline nanoparticles[9,10] have to be added. However, these Electrically Conductive Polymer Composites (ECPCs) have several restrictions. First, the addition of filler particles into the photoresist results in an important increase of the mixture's viscosity. Therefore, during material processing there is a need to control viscosity and sedimentation of filler particles, for example, by additional solvents, which would have a strong influence on photo-polymerization.[9] Second, film deposition on quartz wafers by spin-coating or drop-casting may have a great effect on the surface morphology when using microparticles and may lead to inhomogeneous conductive layers.[11] Due to surface roughness the challenge arises to interpret the conductivity behavior of thin film layers. Third, composite material structuring is constrained to 10–30 μm because of the light diffraction from filler particles.[7,9,11] And finally, cured material has low transparency over the visible range.

Ionic liquids (ILs) have appeared in recent years as novel compounds in materials research and are already used in industrial processes due to several attractive characteristics. They feature high ionic conductivity (up to 30 mS cm^{-1}), low volatility, low flammability, excellent solvent solubility, and high thermal and chemical stability.[12] This new class of materials possesses a wide electrochemical window up to 5.7 V, which describes the potential range in which the IL does not undergo any oxidation or reduction reactions.[13] ILs have the immense advantage of being transparent and easy to produce, with a wide variety of anion/cation combinations which can be adjusted to tailor their physical properties.[14,15] ILs seem to be very promising materials for applications not only in flexible electronic devices, such as displays and photovoltaics[16] but also in electrochemical biosensors because of their good compatibility with biomolecules and enzymes, and even whole cells.[17] Several reviews are available covering the main characteristics of ILs, their advantages, application challenges, and scientific potential.[18–20] A brief qualitative and quantitative overview of established and emerging transparent and conductive materials, including IL–polymer composites, is presented in Table 1 by Loeffelmann et al.[21]

The liquid nature of ILs is an obstacle to applications where a predefined physical shape is required. For these applications, a process of solidification is necessary which enables the immobilization of ions.[15] It comprises the formation of a branched polymer or a 3D solid structure in the form of a polymer matrix, which entraps the IL in the porous network. In this material, liquid-like properties (e.g., charge transport) originate from the IL, whereas solid-like properties originate from the host polymer, which contributes to material flexibility while preventing the system from flowing.

Free radical polymerization is a key method used by the polymer industry to produce a wide range of polymers.[15] During this process polymers are synthesized by linking together monomer units without loss or gain of material due to UV[22] or thermal initiation.[23] There are currently several known IL-polymer combinations that are fabricated by carrying out free radical polymerization of various monomers in IL as solvents or fillers. The influence of ILs on the polymerization kinetics of monomers and their application in photopolymerizable holographic materials were studied in depth by several research groups.[24–27] The properties of ILs, such as solubility, polarity, and viscosity turned out to be the main factor influencing the polymerization rate of the IL-monomer systems.[24, 27,28]

The combination of light-sensitive nonconductive polymers (e.g., SU-8 or IP-L 780), as a host network, with ILs would bring superior advantages in terms of material characteristics. Compatibility with the 2-PP process yields the opportunity to produce high-resolution conductive structures in a single-step process. The combination of IP-L 780 and IL is of particular interest, since no volatile solvents would have to be removed by an additional process step. As no evaporation of solvents after the polymerization would take place, undesired shrinkage and deformation in the structures can be avoided.[29]

Hence, ILs incorporated into polymer matrix seem to be very promising material class for many industrial and scientific applications, for example in temperature and relative humidity (RH) sensors, in terms of transparency, high sensitivity, long-term thermal, chemical, and mechanical stability.[18–20] Temperature and RH are the most frequently measured environmental parameters, which affect most physical, electronic, chemical, mechanical, and biological systems. Certain chemical reactions, biological processes, and electronic circuits perform only within a limited temperature or RH range.

This paper reports a new crosslinkable, conductive, highly transparent composite material based on a photoresist (e.g., IP-L 780 or SU-8) and the IL 1-butyl-3-methylimidazolium dicyanamide (BMIM DCA). The IL-polymer composites possess a good and stable ionic conductivity (up to 10 mS cm^{-1} at room temperature) over a wide frequency bandwidth (1 kHz–1 MHz) and a good transparency (transmission value of 90% for a 170 μm thick cast film). The described two-photon nanolithography enables a single-step process for direct structuring of the material with extremely high resolution (down to 200 nm) and high aspect ratio (up to 1:20). Combining the advantages of both the material and 3D photolithography, a multifunctional sensor with the enhanced ionic conductivity (up to 4 S cm^{-1})

for temperature and RH sensing is demonstrated. Additionally, the material has the ability of mechanical deformation sensing.

2. Results and Discussion

2.1. Identification of a Transparent, Conductive Polymer–IL Composite

The first step of the process development was to identify physically compatible combinations of a suitable photoresist (amenable to 2-PP lithography) and an IL. Compatible mixtures were required to meet the following criteria: homogeneity, no sedimentation or phase separation for the liquid mixture and optical transparency and sufficient mechanical strength for the resultant polymerized material. Based on the experimental results of our previous study, imidazolium- and DCA-based ILs were identified as ideal candidates.[21] It was found that the length of the alkyl side chain at the imidazolium cation of the IL plays a key role for the compatability of IL and polymer. Because of the longer alkyl side chain at the imidazolium ring, the BMIM cation shows a lower polarity than, for example, 1-ethyl-3-methylimidazolium (EMIM) cation. This leads to a better adjustment in polarity between the IL and the monomer before polymerization and as well between the IL and the polymer after polymerization. In addition, the longer alkyl side chain at the BMIM cation is combined with a higher volume of the ion. This, in turn, lowers the Coulomb interaction between the anion and the cation of the IL and enables more interaction between IL and monomer.

During the screening test a series of mixtures were prepared by varying the photoresist/IL weight ratio, using the photoresists IP-L 780 or SU-8 and the ILs including 1-butyl-3-methylimidazolium dicyanamide (BMIM DCA), 1-ethyl-3-methylimidazolium dicyanamide (EMIM DCA), 1-ethyl-3-methylimidazolium bis(trifluoromethylsulfonyl)imide (EMIM TFSI), 1-butyl-3-methylimidazolium hexafluorophosphate (BMIM PF_6), 1-butyl-3-methylimidazolium tetrafluoroborate (BMIM BF_4), 1-ethyl-3-methylimidazolium tricyanomethanide (EMIM TCM), 1-methyl-1-propylpiperidinium bis(trifluoromethylsulfonyl) imide (BMPyrr TFSI), and 1-butyl-1-methylpyrrolidium dicyanamide (BMPyrr DCA). BMIM DCA, EMIM DCA, and EMIM TFSI did not phase separate with IP-L 780, while BMIM DCA, BMPyrr DCA, BMIM PF_6, and BMIM BF_4 remained homogeneous with SU-8. It was further observed that mixtures based on EMIM TCM or BMPyrr TFSI and photoresist (IP-L 780 or SU-8) were not compatible.

To evaluate the polymerized product of each mixture, a droplet (≈10 µL) was deposited on a glass slide and exposed to UV-light (365 nm) for different periods of time. It was observed that only mixtures including BMIM DCA were long-term stable and retained their transparency, regardless of the photoresist used. Acceptable mechanical stability was achieved when the mixture of photoresist/IL was in the ratio 1:1. Therefore, these samples were selected for further characterization (hereafter referred to as Conductive Polymeric material based on a Photoresist and Ionic Liquid 50—CPPLI 50 for short).

For a better understanding of the interaction between the IL and polymer network, ^{1}H NMR measurements have been done on the pristine IL (BMIM DCA), pristine cured and uncured photoresists (IP-L 780 or SU-8), and the composition of cured and uncured CPPLI 50 based on IP-L 780 or SU-8 (spectra are shown in Figure S1, Supporting Information). The measured spectra suggest the absence of chemical reactivity of the IL components with the photoresist before and after the curing process. Analysis of the integrated area ratios and chemical shift of the IL resonances postcuring reveal identical values to the pure IL spectrum precuring, although there is expected line broadening caused by the introduction of the polymer matrix. These values would be expected to vary in the case that a chemical reaction occurred between the IL and the photoresist during the polymerization.

The second step of the process was the characterization of the conductive properties of CPPLI 50. Generally, IL-polymer composites show good ionic transport properties because of a high self-dissociation and ion-transporting ability of the integrated ILs.[24,30,31] A wide array of electrochemical characterization techniques for conducting polymers are available. The most popular techniques in this field are cyclic voltammetry (CV) and impedance spectroscopy (IS).[32,33] CV allows the assessment of the basic transport properties of the material, including oxidation–reduction reactions and applied potentials. During IS, employing an equivalent circuit (i.e., Randles and Ershler models), useful deductions about the properties of a given material are recorded in situ and interfacial effects are determined.

Figure 1A displays two CV cycles of CPPLI 50 based on IP-L 780 (cyclic voltammograms of other compositions with different weight percentage of the photoresist in the IL are presented in Figure S3, Supporting Information). A steep current increment at both reduction and oxidation limits (i.e., cut-off current) was observed, which can be attributed to a decomposition of the IL (BMIM DCA) at the given potential limit range larger than ≈–0.7 and 2.0 V (results not shown). This observation is in full compliance with the publication of Hayyan et al. who described anion oxidation and cation reduction as being responsible for the anodic and cathodic limits observed in ILs.[13] It has to be noted that a presence of impurities, such as water, and a film thickness of the material are of important consideration in voltammetric data.[32,34] An increase in water content can affect the physical and chemical properties of the material and narrow the electrochemical window. With increasing film thickness, the bulk resistance of the material can limit the current flow. Besides, the presence of dissolved gases, such as oxygen or carbon dioxide, may contribute to the background current. Different voltammetric features of scan 2 and scan 3 in the positive potential directions may represent oxidation of water while those at the negative potential confirm a combination of the reduction of oxygen and water.

Ionic conductivity values of CPPLI 50 were obtained from complex impedance measurements, in which a sinusoidal potential wave of varying frequency was applied to the tested sample. It is assumed that with increasing strength of the applied voltage, the ion mobility in the IL-polymer composite is enhanced.[35] The applied voltage supports the breakup of free ion clusters in the IL phase of the material and leads to a higher number of charge carriers, and hence results to a higher conductivity. In order to avoid fluctuations in the measured

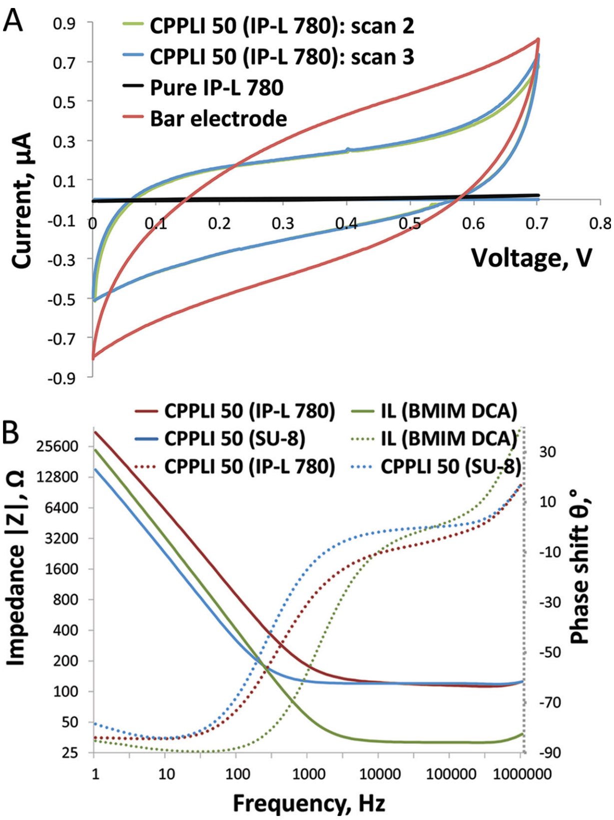

Figure 1. CV of CPPLI 50. A) The current flow was scanned between working glassy carbon and counting platinum electrodes relative to a silver–silver chloride electrode at a frequency $f = 10$ kHz and a scan rate 50 mV s^{-1} at 25.0 °C. The voltammograms for the bare working electrode and pure IP-L 780 are shown for comparison. IS of CPPLI 50. B) The impedance magnitude $|Z|$ was recorded at the voltage amplitude $V = 10$ mV in normal atmosphere for CPPLI 50 based on IP-L 780 (red solid line) and CPPLI 50 based on SU-8 (blue solid line). The corresponding phase angles are shown in red and blue dashed lines. The spectrum for IL (BMIM DCA) is shown for comparison.

conductivity values, caused by the breakup of ion clusters in the IL phase of the material, the measurements were performed at a low voltage of 10 mV.

The impedance spectrum exhibited its maximum value at the lowest frequency and showed an impedance decrease towards higher frequencies until a plateau was reached at ≈1 kHz (red and blue solid lines in Figure 1B). Between 1 kHz and 1 MHz, all spectra showed an almost constant value in the range of 100–200 Ω. It is assumed that at low frequencies, the time intervals between the polarity reversals are sufficiently long for the development of electrical double layers at the interface between the electrode surfaces and the CPPLI structure.[35] In the electrical double layer each layer is conductive, but no significant current can flow between the layers. This accounts for the high impedance values at low frequencies. The strongly negative values of the corresponding phase angles confirmed this assumption (red and blue dashed lines on Figure 1B). They indicated that the system acted similar to a capacitor, where charge is collected at the electrodes. With increasing frequency, the faster polarity reversals counteracted the formation of electrical double layers. Consequently, the impedance spectra exhibited decreasing values. When the corresponding phase angle values strived towards 0°, the system behaved less like a capacitor and more like a resistor.

The conductivity values were calculated according to Equation (S3), Supporting Information. The highest ionic conductivity of the CPPLI 50 based on IP-L 780 was measured to be in the range of 1–10 mS cm^{-1} at a frequency range between 10 kHz and 1 MHz. The value represents a very good ionic conductor behavior for the IL-in-polymer composite.[36–38] For the CPPLI 50 based on SU-8, the ionic conductivity was approximately the same except that the plateau was reached at 1 kHz. One possible explanation of this phenomenon might be a residual solvent. A baking stage precedes the exposure to UV radiation, to remove excess solvents from the layer. Therefore, any remaining solvent may play a role in higher ion transport at lower frequencies.

Optical properties of the material define the ability to transfer or absorb/scatter the light of a certain wavelength. Thus, in the last step of the process spectral sensitivity of the compositions to UV curing was examined by optical spectroscopy. While absorbance spectrum of uncured CPPLI 50 based on IP-L 780 (red solid line in **Figure 2**A) showed high absorbance values (up to 3) between 400 and 450 nm, CPPLI 50 based on SU-8 (blue

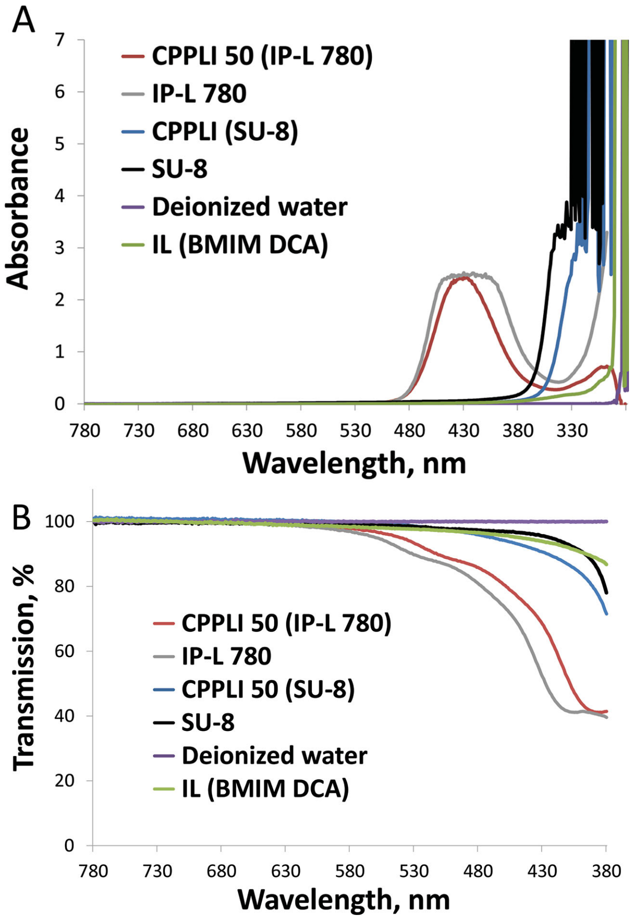

Figure 2. Spectral absorbance of the 170 µm thick layer of uncured CPPLI 50. A) Optical transmission of 170 µm thick cast film of cured CPPLI 50 in the visible spectrum. B) The spectra for pure photoresists (IP-L 780 and SU-8), deionized water, and IL (BMIM DCA) are shown for comparison.

solid line in Figure 2A) demonstrated a significant absorbance increase for wavelengths below 360 nm. A comparison of the CPPLI 50 to pure photoresists' absorbance spectra showed that adding of the IL into the photoresists had no significant influence (i.e., only a slight shift towards lower wavelengths) on the optical properties of the composite materials.

In addition, we examined optical transmission properties of cured CPPLI 50. Both spectra of CPPLI 50 based on IP-L 780 and SU-8 showed high transmission values over nearly the entire visible range between 380 nm and 780 nm (red and blue solid line in Figure 2B). Towards lower wavelengths, a significant transmission decrease was observed for wavelengths below 450 nm (e.g., 80% light transmission for CPPLI 50 based on IP-L 780 and 90% light transmission for CPPLI 50 based on SU-8). This could be detected visually by a slight yellow color of the compositions.

As a result, two IL-polymer composites were identified that address the technical problems of current conductive photolithographic compositions. In contrast to commonly used materials, consisting of crosslinkable materials and filler particles, CPPLI 50 has several advantages: (1) during material handling there is no need to control viscosity and sedimentation of filler particles; accordingly, uniform film deposition can be performed on quartz wafers by spin-coating and drop-casting; (2) material structuring with high resolution is possible due to homogeneity and high clarity of the mixture; (3) and finally, cured material has good optical transparency over the visible range.

Compared to other solid polymer electrolytes, CPPLI 50 has the following benefits: (1) almost no effort with respect to optimizing the material handling has to be performed (e.g., no control of ambient conditions and no special pre- and postprocessing),[36–38] in particular, for CPPLI 50 based on IP-L 780 no care has to be taken to ensure evaporation of solvents before and after polymerization, which would have an effect on mechanical strength and electrochemical stability; (2) it does not contain any plasticizers that are often used to obtain high ionic conductivity (up to 10^{-4} S cm^{-1});[37] (3) it possesses a wide range of material properties (i.e., tunable): the ratio of IL to photoresist can be easily adjusted to tailor physical and chemical properties of the composition (up to 90 wt% of BMIM DCA in the photoresist while remaining completely compatible);[36] (4) cured CPPLI 50 exhibits no ion aggregation of various sizes that is typical for salt-in-polymer electrolytes (e.g., single-ion conductors based on lithium cations).[39]

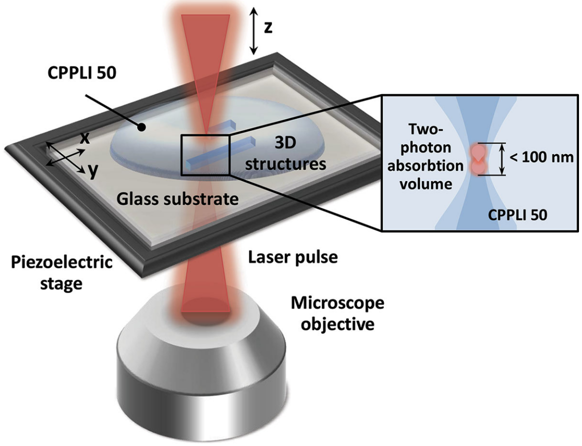

Figure 3. 2-PP photolithography. Left: Schematic illustration of the material curing mechanism by the direct laser writing process. Right: The laser pulse is utilized for spatially confined two-photon absorption volume of the IL–polymer composite inside the focus of the laser beam. A three axis piezoelectrical stage controls the accurate motion of the substrate.

2.2. Two-Photon Nanolithography for Conductive IL–Polymer Composite

After the identification and characterization of the suitable composite mixture, the material was patterned by two-photon nanolithography. Two-photon irradiation leads to a spatially confined power absorption profile within the laser focus, hence triggering photopolymerization of this volume (**Figure 3**). The laser focus trajectory inside the material droplet is defined for computed contours and hatch lines of the 3D structure by scanning the substrate relative to a spatially fixed focal position. Depending on the choice of microscope objective and substrate used, the writing process can be observed in situ and in real-time. Typically, subsequent postexposure thermal treatment leads to chemical crosslinking. After this process, sufficiently crosslinked parts are rendered insoluble in a subsequent developer bath whereas insufficiently or nonexposed parts of the photoresist volume are simply washed away. Finally, the exposed volume is revealed as a freestanding 3D structure. In this context, our goal was the development of a solvent-free IL containing formulation, suitable for the high-resolution 2-PP process. For this reason, we concentrated our attention on CPPLI 50 based on IP-L 780.

The photolithography process was first optimized on a glass slide. We used a 63x magnification (numerical aperture ≤ 1) air objective to have a good vertical resolution. The writing speed was slow enough (100 µm s^{-1}) to achieve complete crosslinking and to guarantee a well-defined geometry and structural rigidity. To ensure that the polymerized material had a good connection to the substrate, and to enhance the mechanical stability, the writing volume overlapped a few micrometers with the substrate.

At the microscale, the electrical properties of the fabricated structures might be influenced not only by the material composition but also by such surface roughness.[40] To evaluate the structures, confocal optical microscopy was used as an intermediate evaluation step before high-resolution scanning electron microscopy (HRSEM). A magnification of 88.000x allowed us to make a detailed investigation of the surface roughness as a function of applied laser power and the direction of writing (i.e., hatching), the distance between polymerized lines and between slices. As examples, the surface roughness of two structures, obtained by writing perpendicular to the length of the structure and using laser powers of 70% and 100%, are depicted in **Figure** 4A,B, respectively. A laser power below 70% was not sufficient for material polymerization. In these examples, the distances between polymerized lines, i.e., wires (Figure 4B), and between the slices of the structures were maintained to be not more than 200 nm, in order to provide

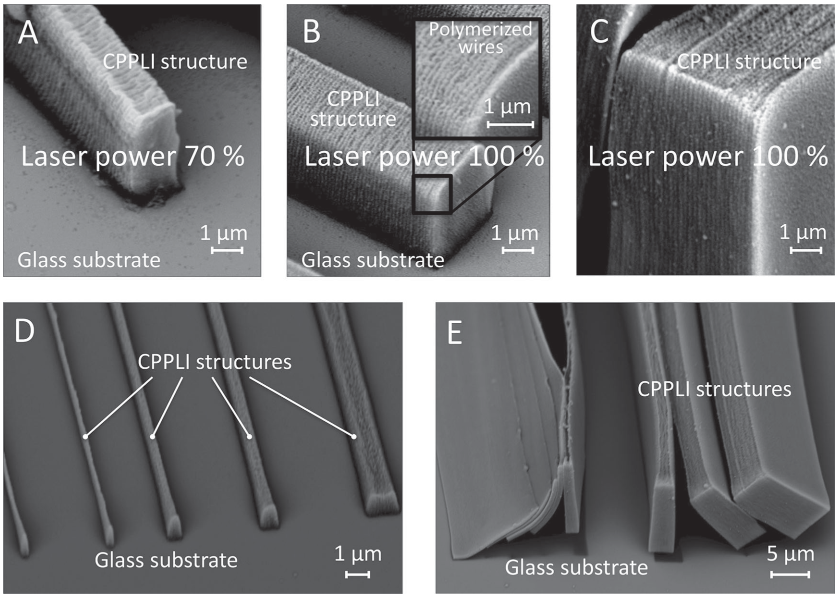

Figure 4. In the upper row, HRSEM images show the surface morphology of the fabricated structures. Different morphologies are displayed resulting from increasing laser power of A) 70% and B) 100% while the direction of laser scanning was perpendicular to the length of the structure. The result of the laser movement along the length of the structure, the laser power of 100%, the distance between scan lines and between slices of 150 nm is presented in (C). In the lower row, HRSEM images of the fabricated conductive line-like structures with a resolution down to D) 200 nm and high aspect ratio up to E) 1:20 are depicted. The distance between scan lines and between slices is 200 nm. The smooth corners of the structures are the result of the ellipsoidal two-photon absorption volume.

smoothness to the crosslinked lines, and to ensure complete interconnection between slices, but not increased further, to avoid development errors due to a lack of intensity. However, it was found that at the applied laser power of 100%, the distance between polymerized lines and between slices could be reduced to below 200 nm to achieve thinner polymerized lines. Figure 4C shows a fabricated structure resulting from a laser power of 100%, hatching parallel to the length of the structure, the distance between cured lines and between slices of 150 nm. A comparison of the CPPLI structures to the pure IP-L 780 structures indicated that adding of the IL to the photoresist has no significant impact on the surface morphology and resolution of the obtained structures (data not shown).

Figure 4D,E show HRSEM images of the fabricated structures with an aspect ratio of 1:20, and a resolution down to 200 nm, achieved with the optimized fabrication parameters. All parameters are listed in Supplementary Material 4, Supporting Information.

For the characterization of the CPPLI structures, we manufactured well-defined microstructures between two metallic electrodes to reduce the writing time, hereafter referred to as sensor elements. The straightforward fabrication process of the electrode substrate used in this work is described in Supplementary Material 5, Supporting Information. A critical aspect in the writing process was to ensure the electrical connection to the electrodes. It was observed that air bubbles, incorporated into the cured CPPLI structure, were the main critical issue. Due to the low wettability of the substrate and the metallic electrodes, tiny air bubbles remained trapped along the perimeter of the electrodes, and at the interface between electrodes and liquid CPPLI (**Figure 5**). To guarantee an electrical contact between the CPPLI structure and the electrodes, the laser had to move over the electrode pad. Consequently, optical reflections from the electrodes caused uncontrolled polymerization and resulted in bubble formation. The electrical characteristics of the sensor element depends on its geometry, hence incorporated air bubbles could make precise quantitative measurements with the small scale sensor elements especially difficult. To prevent non-defined structures during polymerization, two different approaches for electrical interconnection of the sensor element with electrodes were utilized.

The first approach for electrical interconnection included: (1) the manufacturing of a sensor element precisely between the electrodes (i.e., areas of uncontrolled polymerization); (2) generating an additional horizontal overlap (≈5 µm) from both sides of the already polymerized area to the electrodes. The direction of laser movement was fixed along the length of the sensor element to reduce the time the laser spot spent in the potential area of trapped bubbles. These allowed us to dramatically reduce air bubbles embedded inside the sensor element. The geometry of the sensor element, termed sensor element 1, was 200 µm × 10 µm × 10 µm (length × width × height, **Figure 6**A).

The second approach aimed to avoid laser movement over the electrode pad entirely, and included the deposition of conductive polymeric gel-like material between the sensor element and the electrodes by an ink-jet printing process as described by Loeffelmann et al.[35] Figure 6B shows a bracket-like sensor element, named as sensor element 2, with a geometry of 200 µm × 10 µm × 10 µm (length × width × height). The brackets at both ends of the sensor element around the metal electrodes were implemented as capillary traps and helped to ensure the electrical interconnection. By depositing a spreading droplet at the edge of the electrode automatically guaranteed the interconnection with the sensor element without compromising the sensor element. We used a solvent-free ink to minimize problems commonly associated with evaporation during printing (e.g., instabilities caused by increased ink viscosity, nozzle clogging, etc.). A schematic of the ink-jet printing process is depicted in **Figure 7**. It was observed that wetting of the

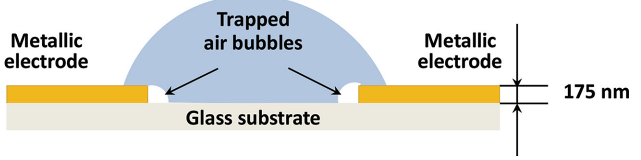

Figure 5. Illustration of air bubbles trapped at the interface between the liquid CPPLI 50 and the electrodes.

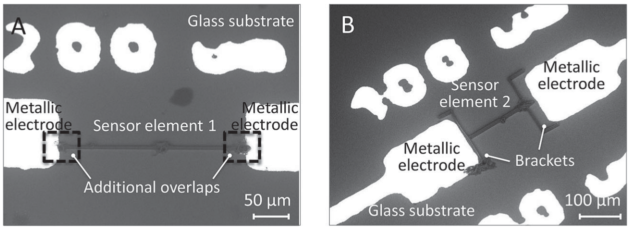

Figure 6. HRSEM images of two sensor elements. A) The geometry of sensor element 1 in terms of length × width × height is 200 µm × 10 µm × 10 µm. The additional horizontal overlaps, indicated by a dashed rectangle, are implemented for the incterconnection of the sensor element and the electrodes. B) The geometry of the sensor element 2 is 200 µm × 10 µm × 10 µm. The brackets at both ends of the structure around the electrodes are implemented as capillary force barriers for ink-jet printing (see Figure 7).

sensor element by ink droplets and droplet accumulation prevented proper electrical contact. To avoid the spreading of the printed fluid, the hydrophobicity of the substrate was increased by silanization (Figure S7, Supporting Information). A silane layer of a few nm prevented spreading and allowed us to control the exact position of each ink-jet printed droplet (i.e., the contact angle was effectively increased from 27° to 75°). As a result, the ink-jet printing of 1 to 15 droplets was sufficient to guarantee the electrical interconnection between the sensor element and the electrodes. Photographs of the sensor element with the ink-jet printed conductive gel-like material are shown as an example in Figure S8, Supporting Information.

The characterization of the conductivity of the two sensor elements was performed by IS. The impedance magnitude |Z| of the two sensor elements was measured as a function of frequency and the graphs are depicted on **Figure 8**. As it can be observed, sensor elements 1 and 2 exhibit a significant difference in their electrical behaviors. It can be assumed that an extra interface (e.g., due to the nm silane layer or the ink-jet printed droplets) produced an additional resistance–capacitance couple, and therefore influenced the electrical characteristics of sensor element 2. The shifting of the corresponding phase angles through the whole frequency range confirmed this assumption.

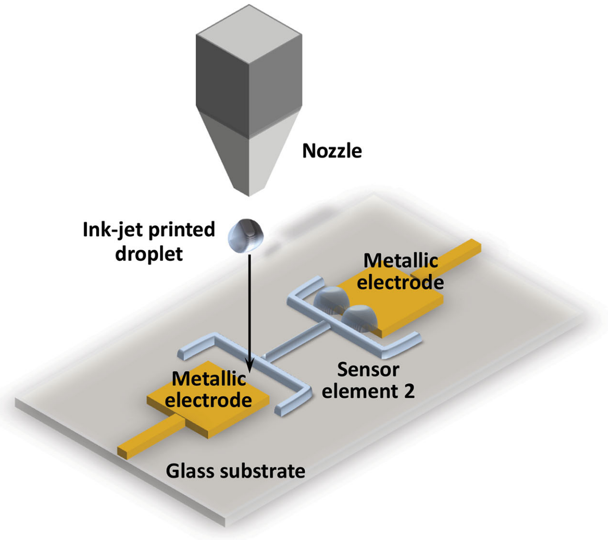

Figure 7. Ink-jet printing process of the solvent-free ink between the sensor element and the electrodes.

A comparison of the fabricated sensor elements and cast specimens (Section 2.1, Figure 2B) clearly indicates that the conductivity of the fabricated microstructures was significantly higher (in the range of 1–4 S cm^{-1}) than those of cast specimens. Moreover, the corresponding impedance phase angles indicate that the sensor element 1 behaves like resistor over the whole range of frequency (1 Hz–1 MHz). We assume that the proposed fabrication method has a strong influence on the CPPLI material characteristics, resulting in enhanced ionic transport at optimal IL concentration and fabrication parameters.

The multilayer structure of the host polymer, identified by HRSEM images, may play a major role in this phenomenon (a schematic illustration is presented in Figure S9, Supporting Information). The ion transport in the crosslinked network is strongly dependent on the interaction between the ions and the polymer matrix. Ion channels (i.e., pores in the polymeric material), established between the cured slices during the 2-PP process, may contain more IL, and therefore may offer pathways for faster ion-conduction. One interesting observation confirms our assumption about the multilayer structure. Delamination of the top slice of a large surface area sample (1 × 1 × 1 mm^3) took place at a laser power of 100%. It is likely that the stress, developed during the curing process, can exceed the limit of plastic deformation of the material.[41] Incomplete polymerization between the slices led to the peeling off of the slice. We thus investigated experimentally the influence of cured slice thickness on conductivity. It was found that by increasing the laser power level from 70% to 100%, cured slices became slightly thinner; however, the conductivity was only marginally affected (in the range of 1%–2%). Conversely, shortening the distance between cured lines and between slices to 150 nm significantly decreased the ionic conductivity (in the range of 12%–15%). The connection between the measured ionic conductivity and the distance between slices suggests that ion transport occurs primarily between the cured slices.

Another possible explanation of enhanced conductivity, supported by the HRSEM images, is that the metal from the electrodes (i.e., gold or chromium) penetrated into the polymeric material during the laser writing process. Metallic particles became incorporated into the sensor element structure and contribute to the electronic conductivity. We noted that the signal (i.e., image intensity), generated from the sensor element in the near-by area of the metallic electrodes, had a similar intensity to that of the electrodes. The huge impedance plateau of sensor element 1 supports this theory. There is no capacitive behavior visible as is typical for ionic conductors (Figure 8).

Although the direct laser writing technology is a very promising manufacturing technique, it is still a developing technology and requires further investigation. In the 2-PP process, various effects occur simultaneously that influence each other and determine the resultant material properties. Only little is known about the crosslinking behavior of the photosensitive monomer and the physical and chemical interactions with IL. The numerous possible driving forces for ion mobility within in a polymer network complicate the predictability of detector

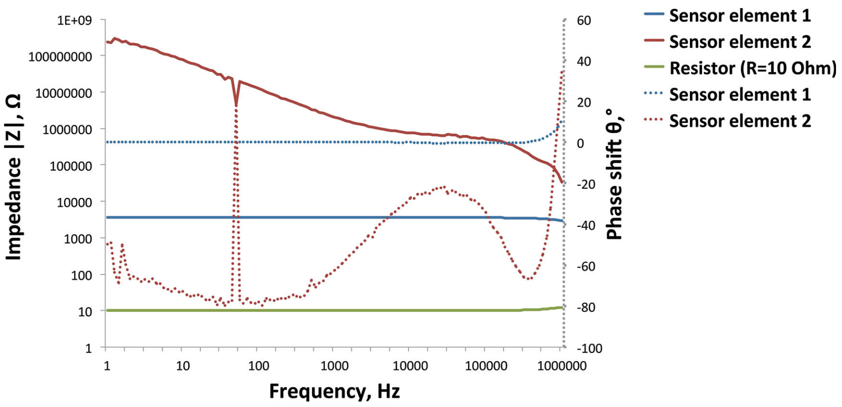

Figure 8. Diagram obtained via electrical IS. The impedance magnitude |Z| as a function of frequency was measured for sensor element 1 (blue solid line) and sensor element 2 (red solid line) in normal atmosphere. The corresponding phase angles are shown in blue and red dashed lines. The spectrum for a 10 Ω commercial resistor is shown for comparison.

performance. Thus, further investigation into the influence of fabrication parameters on the conduction electrochemistry of the CPPLI material is necessary. In particular, attention must be given to different material compositions, also discussed in Supplementary Materials 1 and 2, Supporting Information.

The long sequential writing time of the 2-PP process is a key limitation. An upgrade of the current 2-PP system configuration is claimed to reduce the writing time up to 100 times.[42] This could potentially render the structuring of CPPLI material more practical for applications. Additionally, SU-8 is a commonly used photoresist for the fabrication of advanced semiconductor devices and MEMS. Therefore, the composition based on ILs and SU-8 photoresist is equally applicable for other manufacturing techniques. For example, the combination of conventional and 2-PP photolithography techniques would significantly reduce the writing time while still maintaining the integrity of a complex system.

2.3. Multifunctional Sensor Based on Conductive Polymer–IL Composite

We have described a novel technique for nanolithographic patterning of conductive polymeric structures. These structures are candidates as humidity and temperature microsensors, which typically exploit the variation of electrical conductivity on an environmental quantity. Electrochemical sensors based on ILs benefit from high reproducibility and low cost.[43–45] In fact, similar IL–polymer composite, which was especially developed for the deposition by ink-jet printing, has already been characterized as potential sensing material for temperature and RH measurements.[35] As proof-of-concept, we explored the ionic conductivity change of sensor elements 1 and 2 as a function of temperature or RH change in real time by IS. A photograph of the full sensor is shown in Figure S10, Supporting Information.

In order to investigate the influence of the temperature on the electrical conductivity of the sensor element, the temperature of the surrounding atmosphere was varied while the water content in the desiccator was kept constant. As expected, the conductivity increased with increasing temperature (**Figure 9**A,B). Higher temperatures in the sensor element were coupled with higher mobility resulting in the increase in conductivity.[14,35,45] Compared to sensor 1, sensor 2 exhibited higher sensitivity (up to 0.5 mS cm^{-1} °C^{-1}). This was expected because the total surface area of sensor 2 was larger than that of sensor 1. However, the temperature response linearity (i.e., coefficient of determination R^2) of sensor 1 was superior to sensor 2 ($R^2 = 0.98$ and $R^2 = 0.87$, respectively). The results of the experiments suggest that electronic conductivity is the dominating mechanism for sensor 1. Increasing temperature has a strong influence on ion mobility but almost no effect on electron mobility. The small change of conductivity at high temperatures proves this assumption.

Conductivity as a function of RH was also measured. In Figure 9C,D, conductivity is plotted versus RH at a constant temperature of 23 °C, ranging between 3% and 50% (the level of RH above 50% in the desiccator was not measured because of difficulties in atmosphere control). Sensor 1 responded in a linear fashion to changes in RH. While sensor 2 exhibited higher sensitivity due to increased surface area (up to 0.25 mS cm^{-1} %RH^{-1}), the response was not as linear as sensor 1 ($R^2 = 0.93$ and $R^2 = 0.97$, respectively). One possible explanation of the ionic conductivity change of the sensors in response to different RH levels, supported by Jarosik et al.,[46] might be an increase in the water content in the sensor element. Two possible explanations of this phenomenon may exist.[14,34,35] The first explanation is that the absorbed water decreases viscosity in the system and hence gave rise to increased ionic conductivity due to the higher mobility of the ions. The second explanation is that water dissociates into ions that represent additional charge carriers in the system. Due to a high surface-to-mass ratio of the sensor element, diffusion of water into and out of the structure took place easily.

3. Conclusion

In this paper we have presented novel crosslinkable, conductive, highly transparent materials based on mixtures of photoresists, such as IP-L 780 or SU-8, and the IL BMIM DCA. Almost no additional effort was necessary with respect to optimization of material handling (i.e., purification, ramping of temperature, and controlling of ambient conditions). The lithographic capabilities of the photoresist base material facilitated direct 3D manufacturing of electrically conductive and highly transparent microcomponents by the single-step 2-PP process. The manufacturing process was easily controlled by fast parameter optimization (e.g., scaling, laser power, etc.) in spatial and temporal terms. The successful combination of the developed material with the advanced direct laser writing technique enabled the fabrication of temperature and RH sensor structures. The experimental results demonstrated that the sensors exhibit good sensitivity to a wide range of temperatures (23.0–70.0 °C) and ambient RH (3%–50%).

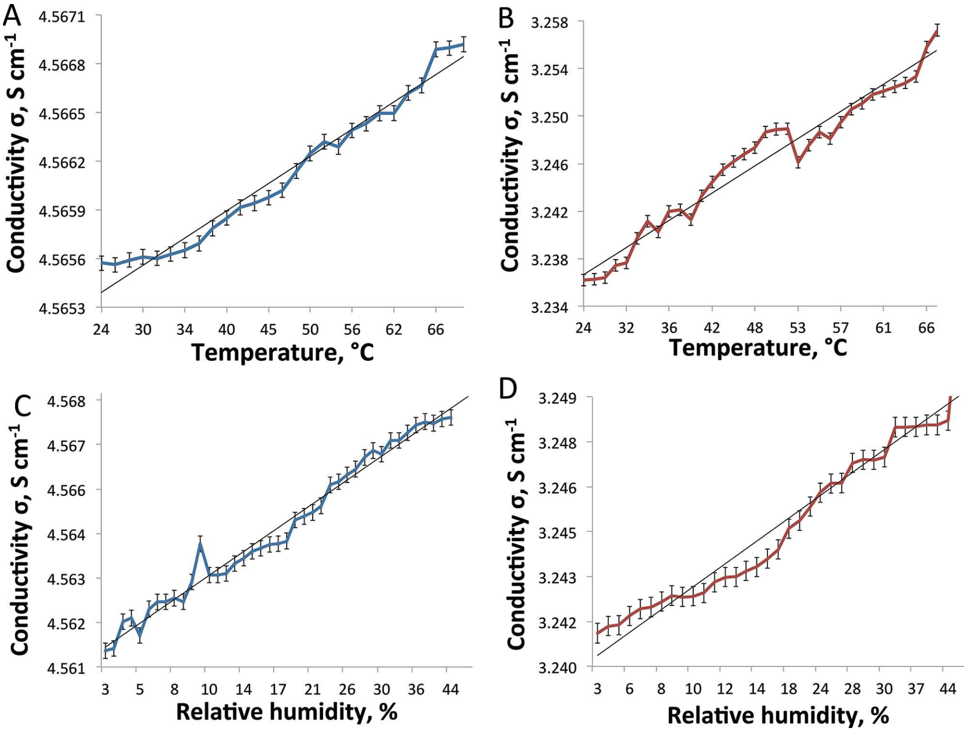

Figure 9. Temperature measurements: ionic conductivity of A) sensor element 1 and B) sensor element 2 as a function of temperature at a RH of 3%. The blue and red lines show the measured values. The black line shows a fitted regression line. RH measurements: ionic conductivity of C) sensor element 1 and D) sensor element 2 as a function of the RH at 23 °C. A sinusoidal signal at a constant potential offset of 10 mV and a frequency of 500 and 700 kHz, respectively, was applied to the tested device, for which the output signal was recorded.

The properties of both photoresist and IL open up a variety of potential applications, such as material for the detection of gases or explosive agents,[20,47,48] in micro- or nanofluidics for in situ tracking and assaying of cells,[5,49,50] etc. For example, the change in ionic conductivity that the material exhibits during deformation could be employed for detecting of biological molecules (Figure S11A, Supporting Information). Mushroom-shaped structures, used by Fendyur et al. for electrical signal read-out from nerve cells,[51] should be able to deliver the full potential of intracellular recording (Figure S11B, Supporting Information). Transparent materials in combination with highly standardized structures can facilitate additional visual control of the cell tracking process and performance of numerous experiments (e.g., electrochemical IS, dielectrophoresis, etc.) in parallel on the same chip with fewer reagents, improved sensitivity, and increased resolution. This will most certainly bring about more precise quantitative and qualitative in vivo analysis for novel true 3D applications in the near future.

4. Experimental Section

Materials and Preparation: Acetone, isopropanol, and trichloro(1H,1H,2H,2H-perfluorooctyl)silane were purchased from Sigma-Aldrich GmbH, Germany. The ILs (e.g., BMIM DCA, >98%, EMIM DCA, >98%, and other ILs) were purchased from IoLiTec, ILs Technologies GmbH, Germany. IP-L 780 and SU-8 3000 series liquid photoresists were used as purchased without further purification from Nanoscribe GmbH, Germany and MicroChem Corp., USA, correspondingly. The preparation of the developed composition was done by manual mixing in a glass vessel. The IL BMIM DCA was added dropwise to the photoresist (IP-L 780 or SU-8). The mixture of components was stirred for a few minutes at room temperature under nitrogen to ensure a homogenous solution. The solution can be stored at room temperature for at least half a year. The solvent-free composition for ink-jet printing contained the IL BMIM DCA, the acrylate monomer 2-(2-ethoxyethoxy)ethyl acrylate (2-(2-EOEO)EA) from Sartomer Europe, France, and the UV initiator Irgacure 1700 (25% bis(2,6-dimethoxybenzoyl)-2,4,4-trimethylpentylphosphine oxide) from Rahn AG, Switzerland as described by Loeffelmann.[35] For the 3D laser writing process a droplet of CPPLI 50 based on IP-L 780 (a volume of a few microliters) was deposited manually on the substrate and was evacuated over night at 0.1 mbar to remove air bubbles from the material.

^{1}H NMR Measurements: ^{1}H NMR spectra of the various components were measured on a Bruker AVANCE III 500 MHz spectrometer (Bruker BioSpin GmbH, Germany) operating at a frequency of 500.12 MHz. For each sample 8 averages each containing 16 K data points were collected over a spectral window of 12 ppm. The resulting FIDs were multiplied with an exponential window function equivalent to 0.3 Hz line broadening prior to Fourier transformation. IP-L 780 or SU-8 was diluted in $CDCl_3$ while IL was measured neat. CPPLI 50 in a 5 mm NMR tube was evacuated over night at 0.1 mbar to remove air bubbles. The sample was measured pre- and post-UV exposure (curing parameters: 365 nm, 1 min interval, 2–5 cycles).

Spectral Absorbance and Optical Transparency: For optical absorbance measurements, a droplet of the material was placed between two quartz glass slides (170 μm thick) and closed from the top. For CPPLI 50 based on SU-8 a step of soft baking at 80 °C for 1 h took place before the measurements. For optical transmission measurements, a 170 μm thick cast film was fabricated the same way and cured under UV-light (365 nm) for 2 min. For CPPLI 50 based on SU-8 a step of postexposure baking at 95 °C for 2 h was required before the measurements. The measurements were performed using a Cary 50 UV–vis spectrometer (Varian Inc., USA).

Electrochemical Characterization: Complex IS was realized using an impedance/gain-phase analyzer (Solartron SI 1260 from Solartron Analytical Ltd., UK) and an electrochemical interface analyzer (Solartron Analytical SI 1287 from Solartron Analytical Ltd., UK), which allowed automatic compensation of the ohmic potential drop. For the measurements of the ionic conductivity, two different setups were used. For the determination of the ionic conductivity of the bulk material, cast cylinders were prepared in UV-transparent polymethylmethacrylate (PMMA) pipe sections (outer diameter 16 mm, inner diameter 12 mm, distance between electrodes 10 mm), and fixed between two stainless steel electrodes. The UV curing was performed by irradiating the sample for different periods of time (3–11 min) at a wavelength of 365 nm through the UV-transparent sidewall. For CPPLI 50 based on SU-8 a step of soft baking at 80 °C for 1 h and a step of postexposure baking at 95 °C for 2 h took place before the measurements. For the ionic conductivity measurements of the sensor, the electrodes were directly contacted with flattened crocodile clamps. The connection to the impedance analyzer consisted of a coaxial Bayonet Neill–Concelman (BNC) cable (impedance $Z = 50\ \Omega$). The impedance analyzer was connected to an external computer and was controlled by ZPlot software. A sinusoidal signal with an amplitude 10 mV was applied over the frequency range from 1 Hz to 1 MHz in normal atmosphere and the impedance spectrum was recorded. Each experiment consisted of 121 measuring points. Data analysis was performed using ZView and Excel Microsoft 2011. CV was realized using a CompactStat portable potentiostat/galvanostat/zero resistance ammeter (ZRA) from Ivium Technologies Inc., USA. The current flow was scanned between working glassy carbon and counting platinum electrodes relative to the reference silver–silver chloride electrode in a neutral buffer at a frequency $f = 10$ kHz and at scan rate 50 mV s^{-1}, starting from anodic to cathodic potentials and reversing back to the initial value. A constant flow rate of nitrogen through the buffer was adjusted manually. The gas flow was supplied to the bath 30 min before the experiments and maintained during the measurements. Once the temperature of the buffer was stabilized at 25.0 °C, the working electrode with a UV-cured droplet (≈3 mm in diameter and 350 µm height) of material was placed in the buffer and the signal was applied over the voltage amplitude range of –0.7 to 2 V. To minimize the influence of regain, three cycles per scan were measured immediately after the working electrode was placed into the buffer. The third cycle was considered for the comparison of the experimental data.

Design Procedure: A 3D computer-aided design program (Solidworks Corp., USA) was used for 3D designs. An original file (*.sldprt) of a 3D solid object was converted into Surface Tesselation Language (STL) for the Nanoscribe Photonic Professional 3D laser lithography system (Nanoscribe GmbH, Germany). Three software packages, Nanoslicer 1.0, DeScribe, and NanoWrite, were used to control the system. To define the structural design, the input STL file was converted by Nanoslicer 1.0 to the Photonic Professional's native data format General Writing Language (GWL), where laser focus trajectories inside photoresist as well as system parameters for the writing process were configured (Supplementary Material 4, Supporting Information). The fabrication parameters for the DLW, such as laser power, laser power scaling, line distance, and scanning speed of the laser focus, were configured in the text editor DeScribe. An example of a GWL code segment can also be found in Supplementary Material 4, Supporting Information. The generated GWL file was loaded straightforwardly by the control software NanoWrite for fabrication.

Temperature and Humidity Measurements: Temperature and RH measurements were carried out in a glass desiccator. The reference temperature and RH levels were measured by a commercial temperature/RH sensor Sensirion SHT 21 (Sensirion AG, Switzerland) in the glass desiccator. Before the temperature measurements, the RH was stabilized at the lowest achievable value (RH = 3%) and at a constant initial room temperature (24 °C). Afterwards, the glass desiccator was heated up on a hot plate (≈0.5 °C $\min^{-1}$), and the change in ionic conductivity was measured by IS as described above. Before the RH measurements, a RH level was also stabilized at the lowest value, then the measurement was started when the reference sensor displayed constant values for at least 1 min. The constant RH value was ensured by simultaneously purging water-free nitrogen and water-containing air into the desiccators (≈0.5% RH $\min^{-1}$). The impedance spectra from the tested device were collected corresponding to the temperature or the RH value from the multifunctional sensor. Calibration measurement of the absorbed moisture from the atmosphere was done prior to RH measurements. The sensor was stored at the beginning in the desiccator at low vacuum and room temperature for at least 2 h. When the sample was taken out of the desiccator, the measurement was done immediately.

HRSEM Imaging: The morphology of the sensing element was characterized by scanning electron microscopy using a high-end desktop microscope Phenom pro X from LOT-Oriel GmbH, Germany. For the investigation of the surface morphology of nonconductive structures, they were sputtered with a few nanometers of gold (Cressington Scientific Instruments Ltd., UK). For imaging of the sensor element a charge reduction sample holder EM–21004 (for nonconductive and low-conductive samples) was used to avoid charging. The acceleration voltage was 10 kV.

Supporting Information

Supporting Information is available from the Wiley Online Library or from the author.

Acknowledgements

N.A.B., N.M., and J.G.K. gratefully acknowledge financial support from the European Research Council (ERC) (Contract Number 290586), which funded this work. We also express our gratitude to the Laboratory for Biomedical Microtechnology (IMTEK, University of Freiburg) for providing access to equipment for IS, the Laboratory for Chemistry and Physics of Interfaces (IMTEK, University of Freiburg); in particular, we are thankful to Samar Kazan and Vitaly Kondrashov for assistance in CV measurements and HRSEM imaging, respectively, and Anton Prohorov (Kiepenheuer-Institute fuer Sonnenphysik (KIS), Freiburg, Germany) for reviewing the paper for theoretical errors related to the field of physics.

Received: December 10, 2014
Revised: January 12, 2015

---

[1] L. R. Harriott, *Proc. IEEE* **2001**, *89*, 366.
[2] A. N. Broers, A. C. F. Hoole, J. M. Ryan, *Microelectron. Eng.* **1996**, *32*, 1.
[3] C. Yu-Tung, L. Tsung-Na, S. C. Yong, Y. Jaemoc, L. Chi-Jen, W. Jun-Yue, W. Cheng-Liang, C. Chen-Wei, H. Tzu-En, H. Yeukuang, S. Qun, Y. Gung-Chian, S. L. Keng, L. Hong-Ming, J. J. Ho, M. Giorgio, *J. Nanotechnol.* **2008**, *19*, 395302.
[4] M. Farsari, M. Vamvakaki, B. N. Chichkov, *J. Opt.* **2010**, *12*, 124001.
[5] R. Wittig, E. Waller, G. von Freymann, *J. Laser Appl.* **2012**, *24*, 042011.
[6] IP-L 780 photoresist datasheet (Nanoscribe, Germany), http://www.nanoscribe.de/en/products/ip-photoresists//html, accessed: February 2014.
[7] R. Abargues, P. J. Rodriguez-Canto, R. Garcia-Calzada, J. Martinez-Pastor, *J. Phys. Chem. C* **2012**, *116*, 17547.
[8] N. Hauptman, M Zveglic, M. Macek, M. K. Gunde, *J. Mater. Sci.* **2009**, *44*, 4625.
[9] S. Jiguet, A. Bertsch, H. Hofmann, P. Renaud, *Adv. Funct. Mater.* **2005**, *15*, 1511.

[10] U. M. Annaiyan, K. Kalantar-zadeh, Q. Fang, I. Cosic, presented at IEEE Tencon 2005, Melbourne, Australia, November **2005**.
[11] M. Benlarbi, L. J. Blum, C. A. Marquette, *Biosens. Bioelectron.* **2012**, *38*, 220.
[12] IoLiTec Ionic, Liquids Technologies Germany, Ionic Liquids Today, http://www.iolitec.de/en/Download-document/665-Ionic_Liquids_Today_01–11.pdf.html, accessed: August 2014.
[13] M. Hayyan, F. S. Mjalli, M. A. Hashim, I. M. Alnashef, T. X. Mei, *J. Ind. Eng. Chem.* **2013**, *19*, 106.
[14] P. N. Tshibangu, S. N. Ndwandwe, E. D. Dikio, *Int. J. Electrochem. Sci.* **2011**, *6*, 2201.
[15] P. Wasserscheid, T. Welton, *Ionic Liquids in Synthesis*, 2nd ed. (Eds: P. Wasserscheid and T. Welton), Wiley-VCH, Weinheim, Germany **2007**.
[16] J. Lewis, *Mater. Today* **2006**, *9*, 38.
[17] F. van Rantwijk, R. A. Sheldon, *Chem. Rev.* **2007**, *107*, 2757.
[18] J. Lu, F. Yan, J. Texter, *Prog. Polym. Sci.* **2009**, *34*, 431.
[19] F. Faridbod, M. R. Ganjali, P. Norouzi, S. Riahi, H. Rashedi, in *Ionic Liquids: Applications and Perspectives* (Ed: A. Kokorin), InTech, Rijeka, Croatia **2011**, Ch. 29.
[20] D. S. Silvester, *Analyst* **2011**, *136*, 4871.
[21] U. Loeffelmann, N. Wang, D. Mager, P. J. Smith, J. G. Korvink, *J. Polym. Sci., Part B: Polym. Phys.* **2012**, *1*, 38.
[22] C. Dietlin, M. Podgorska-Golubska, E. Andrzejewska, *J. Photochem. Photobiol. Chem.* **2014**, *281*, 8.
[23] A. Noda, M. Watanabe, *Electrochim. Acta* **2000**, *45*, 1265.
[24] E. Andrzejewska, M. Podgorska-Golubska, I. Stepniak, M. Andrzejewski, *Polymer* **2009**, *50*, 2040.
[25] S. A. Chesnokov, M. Y. Zakharina, A. S. Shaplov, Y. V. Chechet, E. I. Lozinskaya, O. A. Mel'nik, Y. S. Vygodskii, G. A. Abakumov, *Polym. Int.* **2008**, *57*, 538.
[26] S. A. Chesnokov, M. Y. Zakharina, A. S. Shaplov, E. I. Lozinskaya, I. A. Malyshkina, G. A. Abakumov, F. Vidal, Y. S. Vygodskii, *J. Polym. Sci., Part A: Polym. Chem.* **2010**, *48*, 2388.
[27] H. Zhou, Z. Jiménez, J. A. Pojman, M. S. Paley, C. E. Hoyle, *J. Polym. Sci., Part A: Polym. Chem.* **2008**, *46*, 3766.
[28] H. Lin, P. W. de Oliveira, M. Veith, *Opt. Mater.* **2011**, *33*, 759.
[29] M. Töpper, T. Fischer, T. Baumgartner, H. Reichl, presented at 2010 IEEE Electron. Components Technol. Conf., Las Vegas, USA, June **2010**.
[30] C. Badre, L. Marquant, A. M. Alsayed, L. A. Hough, *Adv. Funct. Mater.* **2012**, *22*, 2723.
[31] M. A. B. H. Susan, T. Kaneko, A. Noda, M. Watanabe, *J. Am. Chem. Soc.* **2005**, *127*, 4976.
[32] H. Matsumoto, in *Electrochemical Aspects of Ionic Liquids* (Ed: H. Ohno), Wiley, Hoboken, NJ, USA **2005**, Ch. 4.
[33] J. Wang, *Analytical Electrochemistry*, Wiley, Hoboken, NJ, USA **2006**.
[34] C. Zhao, G. Burrell, A. A. J. Torriero, F. Separovic, N. F. Dunlop, D. R. Macfarlane, A. M. Bond, *J. Phys. Chem. B* **2008**, *112*, 6923.
[35] U. Loeffelman, *Ph.D. Thesis*, University of Freiburg (Germany) **2014**.
[36] J. Jiang, D. Gao, Z. Li, G. Su, *React. Funct. Polym.* **2006**, *66*, 1141.
[37] C. A. Nguyen, S. Xiong, J. Ma, X. Lu, P. S. Lee, *Phys. Chem.* **2011**, *13*, 13319.
[38] A. S. Fisher, M. B. Khalid, M. Widstrom, P. Kofinas, *J. Power Sources* **2011**, *196*, 9767.
[39] C. G. Joo, L. M. Bronstein, R. L. Karlinsey, J. W. Zwanziger, *Solid State Nucl. Magn. Reson.* **2002**, *22*, 235.
[40] K. M. Ziadan, Conducting polymer application, http://www.intechopen.com/books/new-polymers-for-special-applications/conducting-polymers-application, accessed: August 2014.
[41] J. Bottiger, J. Chevallier, P. Kringhoj, K. O. Schweitz, in *Adhesion Aspects of Thin Films* (Ed: K. L. Mittal), VCP BV, Zeist, The Netherlands **2001**, Ch.1.
[42] Website of the company Nanoscribe http://www.nanoscribe.de//html, accessed: August 2014.
[43] L. Xiong, A. M. Fletcher, S. G. Davies, S. E. Norman, C. Hardacre, R. G. Compton, *Analyst* **2012**, *137*, 4951.
[44] I. Must, U. Johanson, F. Kaasik, I. Poldsalu, A. Punning, A. Aabloo, presented at 2013 IEEE/ASME Int. Conf. on Adv. Intelligent Mechatronics, Wollongong, Australia, July **2013**.
[45] L. Xiong, A. M. Fletcher, S. G. Davies, S. E. Norman, C. Hardacrec, R. G. Compton, *Analyst* **2012**, *137*, 4951.
[46] A. Jarosik, S. R. Krajewski, A. Lewandowski, P. Radzimski, *J. Mol. Liq.* **2006**, *123*, 43.
[47] Y. Liu, M. Tseng, Y. Chu, *Chem. Commun.* **2013**, *49*, 2560.
[48] M. A. G. Zevenbergen, D. Wouters, V. T. Dam, S. H. Brongersma, M. Crego-Calama, *Anal. Chem.* **2011**, *83*, 6300.
[49] S. Kim, F. Qiu, S. Kim, A. Ghanbari, C. Moon, L. Zhang, B. J. Nelson, H. Choi, *Adv. Mater.* **2013**, *25*, 5863.
[50] M. H. Olsen, G. M. Hjorto, M. Hansen, Ö. Met, I. M. Svane, N. B. Larsen, *Lab Chip* **2013**, *13*, 4800.
[51] A. Fendyur, N. Mazurski, J. Shappir, M. E. Spira, *Front. Neuroeng.* **2011**, *4*, 1.